RESEARCH ARTICLE

Effect on Structural, Electrical and Temperature Sensing behavior of Neodymium Doped Bismuth Ferrite

A. K. Sahu[1], Priyambada Mallick[2], S. K. Satpathy[2], Banarji Behera[1,]**

Synthesis of polycrystalline samples of $Bi_{1-x}Nd_xFeO_3$ [x = 0.5, 0.6, 0.7 and 0.8] were demonstrated following solid-state reaction method at high temperature. The structural properties of the sample were confirmed through the X-ray diffraction technique. The dielectric study of the compounds was performed at different frequencies in the range of 100 Hz – 10^6 Hz for various temperatures. The non-Debye type of relaxation process confirmed from impedance analysis. The materials showed a negative temperature coefficient of resistance (NTCR) behavior at various temperatures and frequencies. AC conductivity of the materials with frequency at different temperatures satisfied the universal power law of Johnscher. Thermistor constant (β), sensitivity factor (α), and stability factor for all the samples were calculated and confirmed the characteristics of NTC thermistor.

Introduction

Multiferroic material means the simultaneous existence of two or more Ferroic characteristics namely ferroelectric, ferroelastic or ferromagnetic in the same material [**1**]. The attention to multiferroic materials is now exponentially increasing due to their unique properties and applications which are discussed in a large no of journals [**2,3**]. One of the popular multiferroic materials is Bismuth ferrite ($BiFeO_3$) where both the ferroelectric and ferromagnetic properties exit simultaneously because of the existence of 6s electron lone pair in Bismuth and the partially filled d-orbital of Fe respectively [**4**]. Due to its tremendous physical properties, It can be employed in a various field specifically in multifunctional electronic devices including spintronics, photovoltaic cell, lithium-ion batteries [**5**], transistors, electromagnetic interference filters, [**6**] data storage media, Spin valve devices, non-volatile memory [**7**], multiple state memories, sensors, transducers, actuators [**8**], etc. Nowadays, it is a formidable challenge for the researcher and scientists to synthesize and characterize the Bismuth ferrite [**9**] because of its size effects on the physical properties. There are several synthesis processes to synthesize Bismuth ferrite including the Sonochemical method, Chemical method, sol-gel synthesis, solid-state reaction technique, etc. [**5,10-12**]. But Solid-state reaction technique is cost-effective. Bismuth ferrite has a rhombohedral symmetry and an R3c space group with high Curie temperature (T_C) at 1083 K and Neel temperature (T_N) at 673 K [**13-15**]. There are significant limitations to synthesize single-phase Bismuth Ferrite where current leakage or vacancy of oxygen during sintering is a major problem leading to less ferroelectricity, weak magnetization, in bismuth oxide [**16**]. To overcome the drawback of the single-phase Bismuth Ferrite, research work has been carried out by doping rare earth elements (La, Gd, Nd, Ca, Sm, V, Eu, etc.) [**17,18**] at the A - site of the Ferroic materials to enhance the characteristics of these materials [**19-21**].

Neodymium oxide (Nd_2O_3) is a commonly used important rare earth material for the manufacture of glass, capacitors, and magnets. It is reported that DC conductivity increases and saturation magnetization decrease with an increase in the concentration of Nd_2O_3 with Bismuth Ferrite indicating an ionic contribution to conductivity [**22,23**]. By doping Nd_2O_3 with Bismuth Ferrite, leakage current can be reduced and results in the enhancement of electrical and magnetic properties [**16**]. Also, the resonance frequency will increase with the rising concentration of Nd which can be applicable for radio communication devices [**24-26**]. At higher temperatures, Nd_2O_3 has excellent electrical properties [**27**]. After synthesizing $BiFeO_3$ by the doping of Neodymium through the sol-gel technique, Dawei Wang concluded that the samples transform from the rhombohedral to orthorhombic phase and curie temperature decreases with changing of the Nd concentration in Bismuth Ferrite [**28**]. Furthermore, with increasing the content of Nd, the magnetic and electric properties of Bismuth ferrite are enhanced, while the decrease of

[1]School of Physics, Sambalpur University, Jyoti Vihar, Burla-768019, Odisha, India
[2] School of Applied Physics, Centurion University of Technology and Management, Jatni-752050, Odisha, India

*Corresponding author:
E-mail: banarjibehera@gmail.com; kunuphy.2010@gmail.com;
Tel.: (+91) 9439223383; ORCID ID: 0000-0002-0320-0417

DOI: 10.5185/amlett.2021.071648

dielectric constant and tangent loss are observed [**29,30**]. As the multiferroic $BiFeO_3$ materials show NTCR behavior [**31**], these materials can be utilized in various industry including food, chemical, medicine, automobile, etc. These materials also can be utilized as a temperature sensor, measuring instruments and flow of liquid, liquid level regulator, current and voltage limiters, etc [**32**]. In view of the above, we have elaborately discussed the structural, microstructural, Impendence, ac conductivity, and Thermistor study (parameters) of Neodymium doped Bismuth ferrite $Bi_{1-x}Nd_xFeO_3$ [x = 0.5, 0.6, 0.7and 0.8]

Experimental details

$Bi_{(1-x)}$ Nd_x FeO_3[x = 0.5,0.6,0.7,0.8] were prepared with appropriate stoichiometry content of high purity raw materials i.e., Bi_2O_3 (M/s. CDH, India > 98%), Fe_2O_3 (M/s. CDH, India, > 98.5%), Nd_2O_3 (M/s. Spectrochem, India > 99.9%) through the process of solid-state reaction. First, the oxides were carefully blended in the presence of air atmosphere for 2 h, and then in alcohol for 1h. The blended powders were calcined for 5h at 800 ºC. The calcined powder was then cold-pressed into cylindrical pellets of 10 mm diameter and 1-2 mm of thickness at a pressure of 3.5×10^6 N/m^2 using a hydraulic press. Then the pellets were sintered at 850 ºC for 6 h in an air atmosphere. For the reduction of the brittleness of the pellet, a binding agent Polyvinyl Alcohol (PVA) was introduced. The phase composition and properties of the samples were examined through the XRD process at room temperature using a powder diffractometer (Rigaku, Ultima IV, Japan) by applying the radiation of CuK_α of wavelength λ = 1.5405 Å in a wide range of Bragg's angles 2θ ($20^o \leq 2\theta \leq 80^o$) with a scanning rate of 3º per minute. To demonstrate the electrical properties of the samples, silver air-dying conducting paste is coated on the sintered pellets. After coating, the pellets were heated at 150 ºC for 1 and half hours to remove any moisture and then cooled to room temperature. The impedance parameters were calculated through an LCR meter (HIOKI Model 3532) at a frequency of 10^2 - 10^6 Hz and temperatures in the range of 25 - 450 ºC.

Results and discussion

Structural properties

From the XRD graph in **Fig. 1**, the orthorhombic phase with space group Pmna of all the samples $Bi_{(1-x)}$ Nd_xFeO_3 [x = 0.5,0.6,0.7,0.8] is confirmed at room temperature. For the detailed structural analysis, the XRD data are refined using a ''POWD'' computer program package [**33**]. The size of crystallite (P) is approximately determined using Scherrer's equation, $P = K\lambda/\beta_{1/2}\, cos\theta_{hkl}$ [**34,35**], (where K represents dimensionless shape factor which is nearly equal to 0.89, λ represents X-Ray wavelength of 1.5405Å and $\beta_{1/2}$ = peak width of the broadening line of XRD peak at half of the intensity). The refined lattice parameters and the size ranges of the crystalline are listed in **Table 1**. The average particle size of the samples is in the range of 24-26 nm.

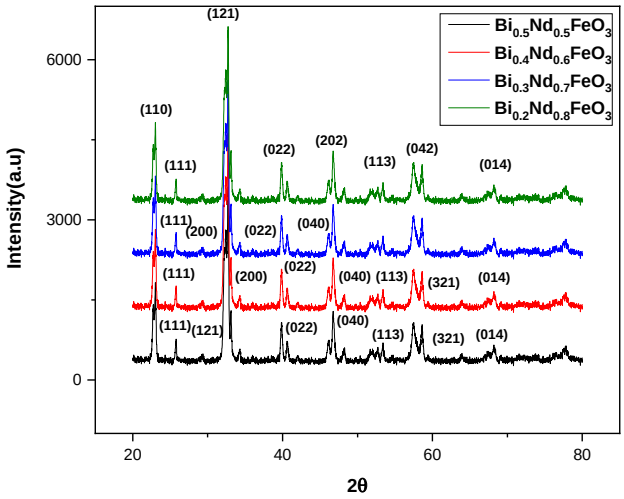

Fig. 1. X-ray diffraction pattern of $Bi_{(1-x)}$ Nd_xFeO_3[x=0.5,0.6,0.7,0.8] and Rietveld Refinement.

Table 1. Comparison of lattice parameters (in Å) and crystal sizes of $Bi_{(1-x)}Nd_xFeO_3$ [x = 0:5, 0.6, 0.7 and 0.8].

	a (Å)	b (Å)	c (Å)	Chi Square	Size of Crystalline (P)
$Bi_{0.5}Nd_{0.5}FeO_3$	5.4280	7.7879	5.5694	5.37	26
$Bi_{0.4}Nd_{0.6}FeO_3$	5.4397	7.7784	5.5790	4.60	24
$Bi_{0.3}Nd_{0.7}FeO3$	5.4418	7.7632	5.5810	4.57	25
$Bi_{0.2}Nd_{0.8}FeO_3$	5.4459	7.7651	5.5791	4.04	24

Microstructural properties

From the SEM micrographs of the sintered pellet at room temperature, densely packed grains are detected over the surface that confirms the polycrystalline nature of the samples. The increase in the concentration of Neodymium does not affect the nature of the grain as shown in **Fig. 2**. The average grain size of the samples cannot be evaluated because of hazy micrographs.

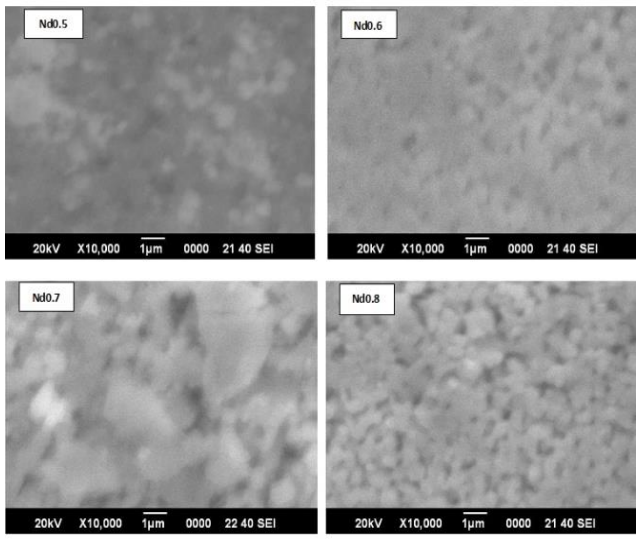

Fig. 2. Scanning Electron Microscope of $Bi_{(1x)}Nd_xFeO_3$ [x = 0.5, 0.6, 0.7, 0.8].

Dielectric study

At different frequencies from the characteristics curve between temperature and the dielectric constant (ε_r), there is a gradual increment of the dielectric constant ε_r with rising temperature but decreases with an increase in frequency (**Fig. 3(a)**). The peak height at the transition temperature is observed to decrease with increasing frequency [**36**]. The anomaly is expected to be present in the sample at a higher temperature region. The value of tangent loss (tanδ) increases with the increment of temperature for all the materials while decreases with rising frequency (**Fig. 3(b)**). It is recognized that the value of tanδ increases with the rising content of Nd. This is due to the improvement in conductivity.

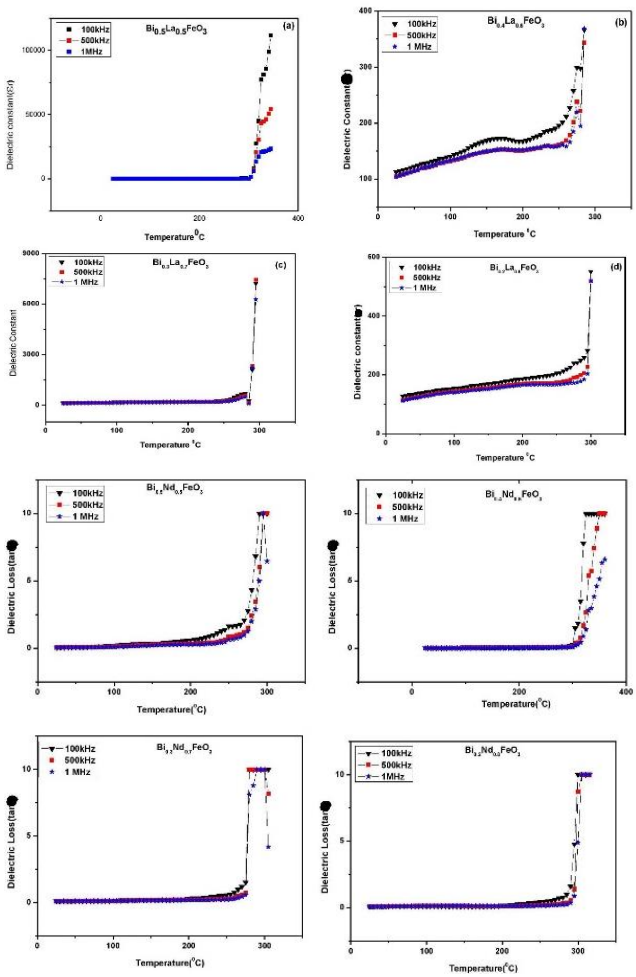

Fig 3 Variation of dielectric constant (ε_r) and dielectric loss (tan δ) of Bi (1-x) Nd x FeO 3 [x=0.5,0.6,0.7,0.8] with temperature at different frequencies

Impedance study

The complex impedance spectroscopy is a unique and powerful tool to investigate the transport characteristics including bulk contribution, grain boundary, and effect of the electrode in the composites [**37**]. The data of electrical ac conductivity for the compounds can be evaluated from the four basic formulas [**38**] which are given as follows:

Complex impedance: $Z^* = Z' - jZ'' = R - \frac{j}{\omega C}$, Complex admittance: $Y^* = Y' + jY'' = \frac{1}{R} + j\omega C$, Complex modulus: $M^* = \frac{1}{\varepsilon^*} = M' + jM'' = j\omega C_0 Z$, Complex permittivity: $\varepsilon^* = \varepsilon' - j\varepsilon''$, Loss tangent, $\tan\delta = \frac{\varepsilon''}{\varepsilon'} = \frac{M''}{M'} = -\frac{Z'}{Z''} = \frac{Y'}{Y''}$.

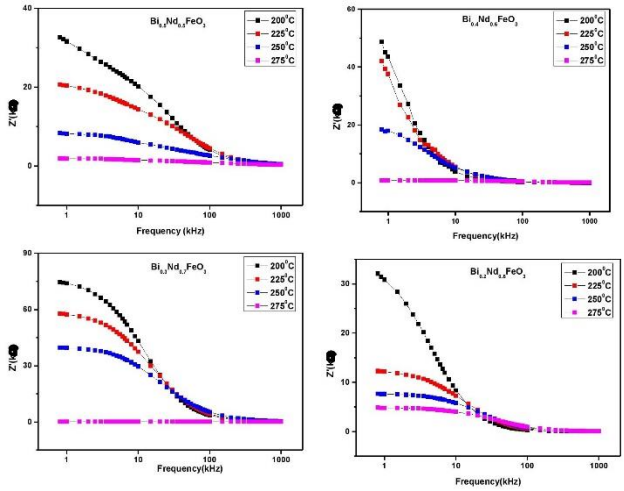

Fig. 4. Variation of Z' as a function of frequency at different temperatures of $Bi_{(1-x)}Nd_xFeO_3$[x=0.5,0.6,0.7,0.8].

The curve between the real part of impedance (Z′) with the frequency at various temperatures in the range of 200-275 °C is shown in **Fig. 4**. It is noticed that the value of the real part of impedance Z' decreases with the rise in temperature indicating the NTCR characteristics. The values of Z' were combined at high frequencies because of the effect of space charge at high temperatures [**39,40**].

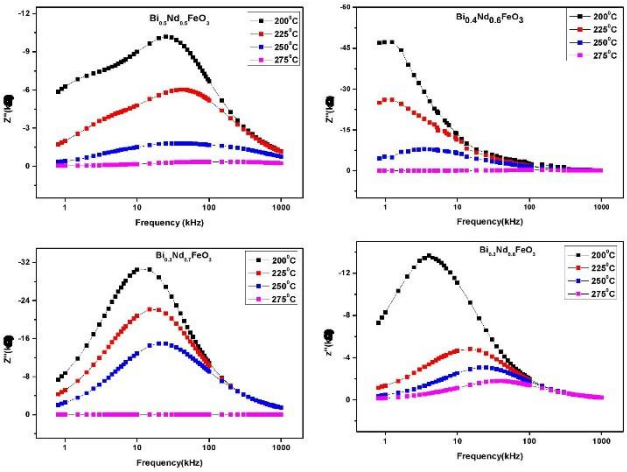

Fig. 5 Variation of Z" as a function of frequency at different temperatures of $Bi_{(1-x)}Nd_xFeO_3$[x=0.5,0.6,0.7,0.8].

The variation of imaginary parts of impedance (Z′) with frequency is shown in **Fig. 5**. The peak position of all the curves deviates towards the region of high frequency that may be observed because of the bulk resistivity or relaxation process. It also may be due to small polaron hopping with minimization of electron–lattice coupling

[**41**]. The characteristic curve between the real part (Z′) and imaginary part Z" of impedance at various temperatures is comprising of an arc centered below the real axis indicating bulk property as shown in **Fig. 6** and follows non-Debye type behavior.

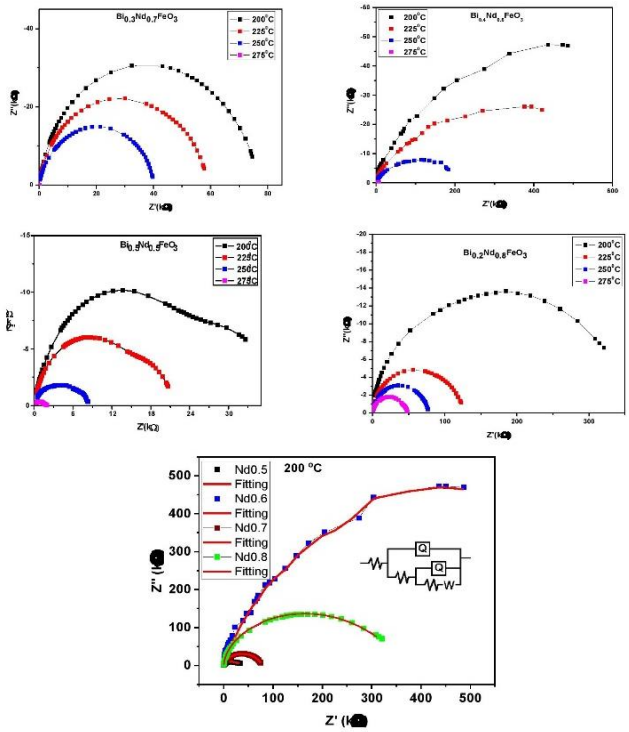

Fig. 6 Complex impedance spectrum (Z′ vs. Z") and experimental and fitted impedance data of $Bi_{(1-x)}Nd_xFeO_3$[x=0.5,0.6,0.7,0.8] at selected temperatures with equivalent circuits (inset).

The Constant Phase Element (CPE) value has been obtained from the Nyquist plot fitting by using ZSimpWin Software which is used in equivalent circuit modeling and data fitting of electrochemical impedance spectroscopy data. The equivalent circuit fitted with R(Q(R(Q(RW)))) as shown in **Fig. 6** for the $Bi_{1-x}Nd_xFeO_3$ [x = 0.5,0.6,0.7 and 0.8] to explain the series of interconnected grain and phenomenon of the grain boundary. The different parameters of the equivalent circuit are given in **Table 2**.

Conductivity

From the ac conductivity (σ_{ac}) vs frequency curve at various temperatures, as shown in **Fig. 7**, the plateaus of ac conductivity (σ_{ac}) are noticed at low frequencies and high temperatures. These frequency-independent values of σ_{ac} indicate the dc conductivity which can be determined using the universal power-law equation of Johnscher [**42**], $\sigma(\omega) = \sigma_{dc} + A\omega^n$, where the term $A\omega^n$ corresponds to the ac dependence describing all the phenomenon of dispersion and the value of 'n' differ from material to material that can be obtained from the fitting parameters as mentioned in **Table 3**.

The ac conductivity (σ_{ac}) of all the samples rises with an increment of temperatures. At high temperatures, the values of ac conductivity combined indicating frequency-independent i.e. dc conductivity [**43-45**].

Table 2. Values of parameters of equivalent circuit of $Bi_{(1-x)}Nd_xFeO_3$ [x = 0.5,0.6,0.7,0.8] at 200^{0}C.

Parameters	X = 0.5	X = 0.6	X = 0.7	X = 0.8
R_1	3.147E+001	1.089E-002	8.542E+001	2.398E+002
CPE or Q_1	1.118E-009	8.511E-008	4.083E-010	2.659E-006
Frequency power (n)	8.609E-001	1.132E-008	9.157E-001	1.375E-011
R_2	3.062E+002	1.903E+002	6.158E+004	1.000E-002
CPE or Q_2	2.255E-003	6.414E-008	5.894E-008	8.099E-011
R_3	4.377E+004	1.016E-001	1.648E+004	7.247E+005
Frequency power (n)	1.928E-011	8.000E-001	6.188E-001	9.928E-001
W	1.746E-007	1.000E-020	5.914E+005	7.693E-009
Chi square	1.077e-04	1.836e-02	4.390e-05	4.974e-04

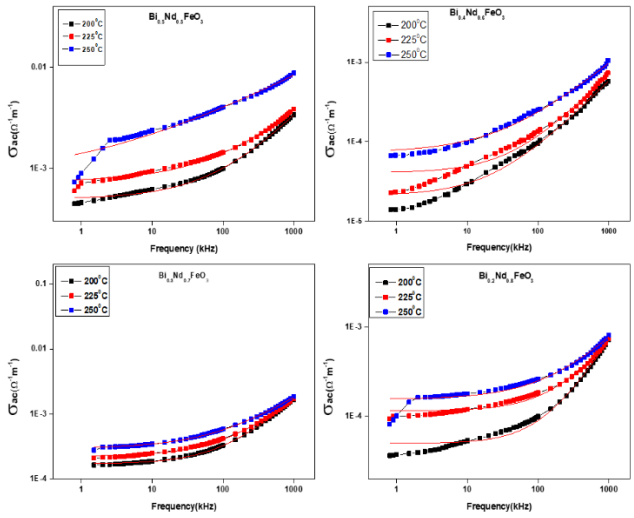

Fig. 7. Variation of ac conductivity (σ_{ac}) of $Bi_{(1-x)}Nd_xFeO_3$ [x = 0.5, 0.6, 0.7, 0.8] with frequency at different temperatures.

Table 3. Fitting parameters obtained from the Jonscher power law at different temperatures.

	$Bi_{0.5}Nd_{0.5}FeO_3$			$Bi_{0.4}Nd_{0.6}FeO_3$			$Bi_{0.3}Nd_{0.7}FeO_3$			$Bi_{0.2}Nd_{0.8}FeO_3$		
T^{0}C	σ_{dc}	A	n	σ_{dc}	A	n	σ_{dc}	A	n	σ_{dc}	A	n
200^{0}C	5.00206E-4	8.7241E-8	0.75321	2.09642E-5	2.36381E-9	0.8965	-0.00706	9.06688E-5	0.52222	5.00039E-5	3.52014E-11	1.21169
225^{0}C	7.43398E-4	3.84167E-7	0.64961	4.05697E-5	1.58816E-9	0.93978	1.70261E-4	1.84925E-9	0.98512	1.15061E-4	3.26417E-10	1.04379
250^{0}C	8.20989E-4	4.59889E-5	0.36917	7.36679E-5	3.27942E-8	0.74005	2.2378E-4	5.37037E-9	0.90652	1.55704E-4	7.83372E-9	0.81649
275^{0}C	-0.00534	0.00187	0.2095	0.00163	2.07094E-8	0.85493	2.96146E-4	5.36138E-8	0.74195	1.90713E-4	3.43872E-7	0.56218

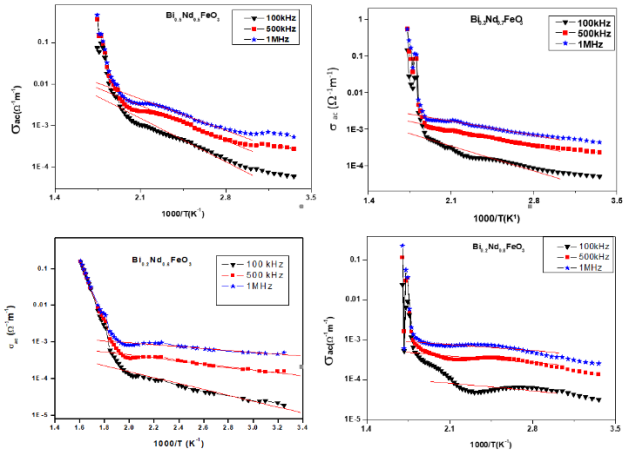

Fig. 8. Variation of ac conductivity (σ_{ac}) with (10^3/T) of $Bi_{(1-x)}Nd_xFeO_3$[x = 0.5,0.6,0.7,0.8].

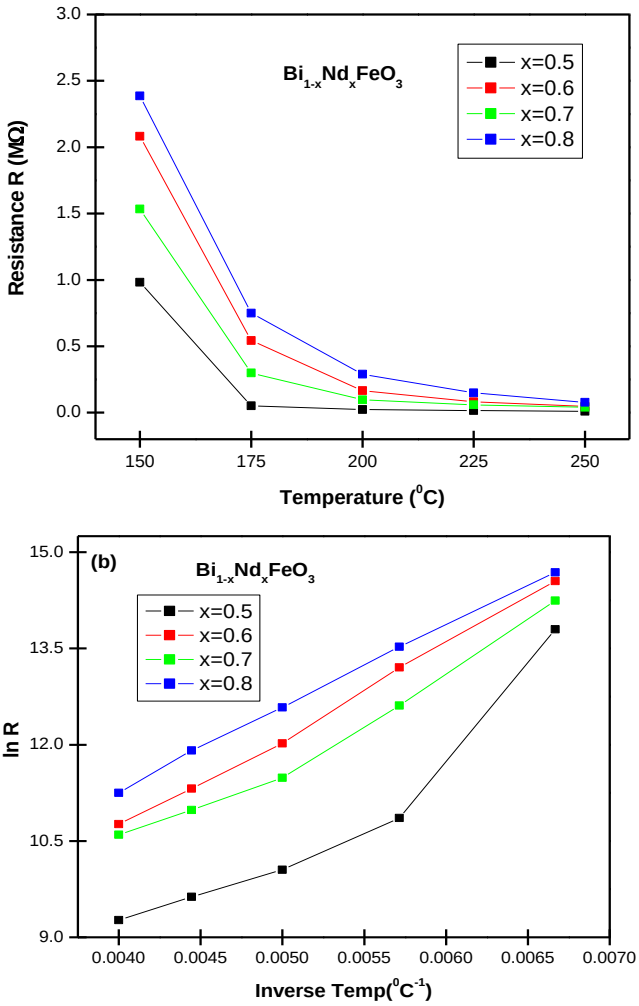

Fig. 9. Variation of Resistance R with Temperature T and logarithmic R with Temperature T of $Bi_{(1-x)}Nd_xFeO_3$[x = 0.5,0.6,0.7,0.8].

Electrical resistance

The electrical resistance of samples $Bi_{(1-x)}$ Nd_x FeO_3[x=0.5,0.6,0.7 and 0.8] are determined at different temperatures. The exponential variation of resistance of the samples with different temperatures ranging from 175^{0}C to 250^{0}C confirms the NTCR behavior [**46,47**] of samples as shown in **Fig. 9(a)**. It is observed that the value of resistance increases with the increase of Nd concentration in BFO and indicates the transformation of the state of conductive to insulating state [**48**].

Electrical resistance (R) of NTC thermistors can be explained as a function of temperature which is related by the equation $R_T = \exp\left(\frac{1}{T}\right)$. It can be also simplified as $ln(R_T) = \frac{1}{T} + C$, where R_T represents the resistance of the sample at respective temperature T. The variation between logarithmic resistance and the inverse temperature is linear as shown in **Fig. 9(b)**. This linearity behavior of samples explained the excellent NTCR characteristics that can be useful in the high-temperature thermistor including the temperature sensor. The deviation in graphs for some samples was aroused because of systematic errors of processing parameters, the effect of sintering, and doping contents.

Thermistor constant (β)

Thermistor constant (β) can be determined from the relation between electrical resistance and temperature which is given by $\beta = ln\left(\frac{R_1}{R_2}\right) \Big/ \frac{1}{T_1} - \frac{1}{T_2}$. It is found that NTCR thermistors follow the equation of Arrhenius in the temperature range of 175 - 250 °C. The β values of all the compositions at different temperatures are mentioned in **Table 3**.

For NTC thermistor, the thermistor constant (β) is closely related to electrical resistance (R) and temperature (T) by the relation $R = exp\left(\frac{\beta}{T}\right)$. The above equation indicates linearity characteristics between thermistor constant β and the natural logarithm resistance (R) satisfying the Arrhenius equation [**32**] as noticed in **Fig. 10**. Because of these linear relations, it can be useful for biomedical and medical applications, thermistor-based devices, temperature sensors, etc. [**29**].

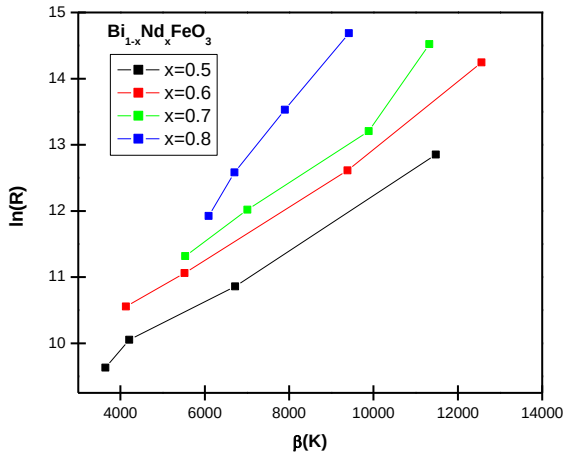

Fig. 10. Variation of logarithmic of resistance with β(K) of $Bi_{(1-x)}Nd_xFeO_3$[x = 0.5,0.6,0.7,0.8].

Table. 4. Concentration dependent thermistor constant(β), activation energy(E_a) and sensitivity index(α) of BNF ceramic.

Measuring temperature (℃)	Sintering Temperature 850^{0}C											
	$Bi_{0.5}Nd_{0.5}FeO_3$			$Bi_{0.4}Nd_{0.6}FeO_3$			$Bi_{0.3}Nd_{0.7}FeO_3$			$Bi_{0.2}Nd_{0.8}FeO_3$		
	β	E_a	α	β	E_a	α	β	E_a	α	β	E_a	α
175	8417.895	0.7254	-0.0470	12563.23	1.08261	-0.07021	10326.47	0.8898	-0.05771	9414.911	0.8113	-0.05262
200	6721.996	0.5792	-0.0334	9386.672	0.80888	-0.04677	9887.316	0.8520	-0.04926	7901.24	0.6808	-0.03937
225	4209.274	0.3627	-0.0188	4996.794	0.43059	-0.02233	7013.656	0.6043	-0.03135	6703.36	0.5776	-0.02996
250	3647.04	0.3142	-0.0147	3851.207	0.33187	-0.01553	5536.62	0.47711	-0.02232	6576.421	0.56671	-0.02652

Temperature coefficient of resistance

The value of sensitivity index or temperature coefficient of resistance (α) can be determined from the value of thermistor constant β using the relation of Steinhart–Hart coefficient $\beta = \sqrt{\left(\frac{b}{3c}\right)^3 + \frac{\alpha^2}{4}}$ [**46**] which can be simplified as $\alpha = \frac{a-T}{c} = \frac{-\beta}{T^2}$. It is confirmed that α decreases with rising in thermistor constant β [**49**] as shown in Table 3. The sensitivity index (α) is generally described in percentage per degree centigrade (%/℃) [**47**].

Sensitivity

The sensitivity of an NTC thermistor can be explained by its sensitivity index (α) and activation energy (E_a) as shown in **Table 4** for the different content of dopant Nd in BFO. The sensitivity of the composites decreases up to x=0.6 in $Bi_{1-x}Nd_xFeO_3$; but it rises unexpectedly at x = 0.7. These variations of sensitivity may be due to the existence of extrinsic charge carriers in grain.

Stability factor

The stability factor can be determined by using simple relation which is equal to the ratio of highest to the lowest value of resistance. As the content of dopant Nd rises in BFO, the stability factor of all the materials decreases. Based on the above explanation, it is confirmed that Nd-doped BFO is a suitable material for NTC thermistors with better performance and stability factors as shown in **Table 5**.

Table 5. Stability factor at different concentration of Nd.

Doping concentration of Nd	R_{max}/R_{min}	Stability factor $log(R_{max}/R_{min})$
x = 0.5	92.9802	1.9683
x = 0.6	58.72616	1.76883
x = 0.7	43.989308	1.64334
x = 0.8	30.9588	1.490785

Conclusion

$Bi_{(1-x)}$ Nd_x FeO_3[x=0.5,0.6,0.7 and 0.8] composites were synthesized using a solid-state reaction technique and the orthorhombic structure with space group Pmna. The average crystallite sizes of the samples are in the range of 24-26 nm. The dielectric constant of all the samples increases with a rise in temperature. The Nyquist plot reveals the contribution of the bulk characteristics in the materials. AC conductivity study with frequency obeys the power law. The linearity relationship between logarithmic resistance and the inverse temperature is observed that confirms the NTC thermistor properties. On the increment of dopant Nd content, its stability factor decreases. All the materials showed NTCR behavior. Due to the above excellent NTCR behavior, it can be applicable in temperature sensors, thermistor-based electrical devices, etc.

Acknowledgments

The authors are thankful for the financial support through DRS-I of UGC under SAP and FIST Programme of DST for the development of research work in the School of Physics, Sambalpur University, and the DST under SERC Fast Track Scheme for Young Scientist (Project No. SR/FTP/PS-036/2011) New Delhi, India.

Conflicts of interest
There are no conflicts to declare.

Keywords

Solid-state reaction, XRD, electrical conductivity, thermistor constant, NTCR behavior.

Received: 11 February 2021
Revised: 3 April 2021
Accepted: 26 April 2021

References

1. Wang, J.; Science, **2003**, *299*, 1719.
2. Manjunatha, K.; Jagadeesha Angadi, V.; Srinivasamurthy, K. M.; Matteppanavar, S.; Pattar, V. K.; Mahaboob Pasha, U.; *J. Supercond. Nov. Magn.*, **2020**, *33*, 1747.
3. Hamrita, A.; *Ceram. Int.*, **2014**, *40*, 1, 1461.
4. Wu, H.; Zhou, J.; Liang, L.; Li, L.; Zhu, X.; *J. Nanomater.*, **2014**, *2014*.
5. Slimani, Y.; *J. Mater. Sci. Mater. Electron.*, **2020,** *31*, 7786.
6. Hill, N. A.; Filippetti, A.; *J. Magn. Magn. Mater.*, **2002**, *242*, 976.
7. F. M.; Spaldin N.A.; *Science*, **2005**, *309*, 391.
8. Irfan S.; J. Mat,er. Res. Technol., **2019**, *8*, 6, 6375.
9. Mostafavi E.; Ataie A.; Ahmadzadeh M.; *Adv. Mater. Res.*, **2014**, *829*, 683.
10. Slimani, Y.; *Ultrason. Sonochem.*, **2019**, *59*.
11. Slimani, Y.; *Ultrason. Sonochem.*, **2019**, *57*, 203.
12. Almessiere, M. A.; Slimani, Y.; Baykal, A.; *J. Alloys Compd.*, **2018**, *762*, 389.
13. Kubel F.; Schmid H.; *Acta Crystallogr. Sect. B*, **1990**, *46*, 698.
14. Michel C.; Moreau J. M.; Achenbach G. D.; James W. J.; *Soli State Commun.*, **1969**, *7*, 9, 701.

15. Fischer P.; Polomska M.; Sosnowska I.; Szymanski M.; *J. Phys. C Solid State Phys.*, **1980**, *13*, 10, 1931.
16. Maleki H.; *J. Mag. Mag. Mat.*, **2018**, 1–18.
17. Almessiere, M. A.; Slimani, Y.; Baykal, A.; *J. Alloys Compd.*, **2018**, *767*, 966.
18. Almessiere, M. A.; *Ultrason. Sonochem.*, **2019**, *58*, 104621.
19. Lomanova, N. A.; *Russ. J. Gen. Chem.*, **2019**, *89*, 1843.
20. Sahu, A. K.; Satpathy, S. K.; Rout, S. K.; Behera, B.; *Trans. Electr. Electron. Mater.*, **2020**, *21*, 2, 217.
21. Yan, Z.; Wang, K. F.; Qu, J. F.; Wang, Y.; Song, Z. T.; Feng, S. L.; *Appl. Phys. Lett.*, **2007**, *91*, 13.
22. Pan, T. M.; Der Lee, J.; Shu, W. H.; Te Chen, T.; *Appl. Phys. Lett.*, **2006**, *89*, 23, 18.
23. Basu, S.; Mukherjee, A.; Houssain, S. M.; Pal, M.; *Proc. Int. Conf. Nanosci. Eng. Technol.*, **2011**, *228*.
24. Almessiere, M. A.; *J. Mater. Res. Technol.*, **2020**, *9*, 11278.
25. Almessiere, M. A.; *Ceram. Int.*, **2020**, *46*, 7346.
26. Almessiere, M. A.; Genc, F.; Sozeri, H.; Baykal, A.; Trukhanov, S. V.; Trukhanov, A. V.; *J. Mater. Sci. Mater. Electron.*, **2019**, *30*, 6776.
27. Ali, A. A.; Shaaban, M. H.; *Solid State Sci.*, **2010**, *12*, 2148.
28. Wang, D.; *Ceram. Int.*, **2015**, *41*, 8768.
29. Kumar, A.; Sharma, P.; Varshney, D.; *J. Ceram.*, **2015**, *2015*, 1.
30. Li, Y.; Cao, W. Q.; Yuan, J.; Wang, D. W.; Cao, M. S.; *J. Mater. Chem. C*, **2015**, *3*, 9276.
31. Yuan, C. L.; Liu, X. Y.; Xu, J. W.; Zhang, X. W.; Zhou, C. R.; *Bull. Mater. Sci.*, **2012**, *35*, 425.
32. Nenova, Z. P.; Nenov, T. G.; *IEEE Trans. Instrum. Meas.*, **2009**, 58, 441.
33. Wu, E.; *Acta Cryst.*, **1989**, *1988*, 506.
34. Scherrer, P.; Mathematisch-Physikalische Klasse. **1918**, *2*, 98.
35. Klug, H.P.; Alexander, L.E.; X-ray diffraction procedures for Polycrystalline and Amorphous Materials, Willey-Interscience, New York, 1974.
36. Chowdari, B. V. R.; Gopalakrishnan, R.; *Solid State Ionics*, **1987**, *23*, 225.
37. Naushin, N.; Md Shahriar, S.; Roy, O.; Sharif, A.; *J. Eng. Sci.*, **2020**, *11*, 123.
38. Fang, J.; Wang, J.; Ng, S. C.; Gan, L. M.; Quek, C. H.; Chew, C. H.; *Mater. Lett.*, **1998**, *36*, 179.
39. Płcharski, J.; Weiczorek, W.; *Solid State Ionics*, **1988**, *28*, 979.
40. Ted Kroon, R. E.; *S. Afr. J. Sci.*, **2013**, *109*, 5.
41. Cao, W.; Gerhardt, R.; *Solid State Ionics*, **1990,** *42*, 213.
42. Jonscher, A.K.; *Nat. Publ. Gr.*, **1977**, *267*, 673.
43. Satpathy, S. K.; Mohanty, N. K.; Behera, A. K.; Sen, S.; Behera, B.; Nayak, P.; J. Electron. Mater., **2015**, *44*, 4290.
44. Satpathy, S. K.; Mohanty, N. K.; Behera, A. K.; Behera, B.; *Mater. Sci. Pol.*, **2014**, *32*, 59.
45. Sahoo, S.; *J. Adv. Ceram.*, **2018**, *7*, 99.
46. Jadhav, R. N.; Mathad, S. N.; Puri, V.; *Ceram. Int.*, **2012**, *38*, 5181.
47. Sahoo, S.; Parashar, S. K. S.; Ali, S. M.; *J. Adv. Ceram.*, **2014**, 2, 117.
48. De Vasconcelos, E. A.; Khan, S. A.; Zhang, W. Y.; Uchida, H.; Katsube, T.; *Sensors Actuators, A Phys.*, **2000**, *83*, 167.
49. Yuan, C.; Liu, X.; Liang, M.; Zhou, C.; Wang, H.; *Sensors Actuators, A Phys.*, **2011**, *167*, 291.

Authors biography

Mr. Akshaya Ku. Sahu currently works as a lecturer in the Department of Physics, Barpalli College, Barpalli, Bargarh, Odisha. His current areas of research are Ferroelectrics, Advanced Materials, Multiferroics, Composites, and other ceramic materials. He is currently pursuing her Ph.D. in Physics at Sambalpur University, Sambalpur, Odisha, India.

Ms. Priyambada Mallick is currently pursuing her Ph.D. in Physics at Centurion University of Technology and Management (CUTM), Odisha, India. Her current area of researches are Ferroelectrics, Advanced materials, Perovskite materials based on the energy storage device. She has completed her Bachelor of Science (Physics) in 2015 at Bhadrak Autonomous College, Bhadrak, Odisha, and Master's degree (Physics) in 2017 at Fakir Mohan University, Balasore, Odisha, India. She has received her M.Phil. degree (Physics) in 2019 from Ravenshaw University, Cuttack, Odisha. She has qualified for CSIR NET LS in December 2018 and also qualified for GATE 2019.
Mail id: priyambadamallick17@gmail.com, 190506162007@cutm.ac.in

Dr. Santosh Kumar Satpathy currently works as an Assistant Professor in the Department of Physics, School of Applied Sciences, Centurion University of Technology and Management, Odisha, India. He has completed his M.Sc. (Physics) from Sambalpur University. He has received his M.Phil. in Physics from the School of Physics, Sambalpur University, India. He has completed his Ph.D. from Sambalpur University in collaboration with Central Glass & Ceramic Research Institute, Kolkata. He has more than 26 research papers in different international and national journals. Six (6) M.Phil. students have been awarded and three (3) students are continuing Ph.D. under his guidance. He had gained some expertise in the field of nano structuration of polymer systems confined in thin films in combination with reactive polymers. The present expertise in the field of nanostructured materials boost his faith and enabled him to carry forward in the field of high-energy storage devices. Now he is working in the field of ferroelectric, multiferroic, optical properties, and magnetic properties for the application of energy storage materials, believed to produce outcomes which purposeful from the industrial point of view, as well as from laboratory scale to large scale implementation in the field of miniaturization of nano-scale industry and fabrication of flexible thin-film capacitors for advanced energy storage. He is a life member of Orissa Physical Society. Mail id: santosh.satpathy@cutm.ac.in, kunuphy.2010@gmail.com

Dr. Banarji Behera Ph.D. from Sambalpur University in collaboration with the Indian Institute of Technology (IIT), Kharagpur is presently a Reader at the School of Physics, Sambalpur University, Jyoti Vihar, Burla, Sambalpur, Odisha, India. He has more than 11 years of teaching and 15 years of research experience. His current areas of research are Ferroelectrics, Advanced Materials, Multiferroics, Composites, and other ceramic materials. He has more than 100 research papers in international journals and 12 conference proceedings. He had visited UNESP, Sao Paulo, Brazil for one and half years as Postdoctoral Fellow. Twenty (20) M.Phil. students and six (07) Ph.D. students have been awarded under his guidance. He has organized 03 National Seminars and delivers 10 invited talks in different national conferences/seminars/workshops.
Mail id: banarjibehera@gmail.com